



Solution NMR studies of the plant peptide hormone CEP inform function



Benjamin G. Bobay^{a,1}, Peter DiGennaro^{b,1}, Elizabeth Scholl^b, Nijat Imin^c,
Michael A. Djordjevic^c, David Mck Bird^{b,d,*}

^a Department of Molecular and Structural Biochemistry, NC State University, Raleigh, NC 27695, United States

^b Department of Plant Pathology, NC State University, Raleigh, NC 27695, United States

^c Plant Science Division, Research School of Biology, College of Medicine, Biology and Environment, The Australian National University, Canberra ACT 0200, Australia

^d Bioinformatics Research Center, NC State University, Raleigh, NC 27695, United States

ARTICLE INFO

Article history:

Received 26 August 2013

Revised 14 October 2013

Accepted 24 October 2013

Available online 5 November 2013

Edited by Michael R. Sussman

Keywords:

NMR

Molecular dynamic

CEP

Root-knot nematode

Peptide

CLE

Meloidogyne

ABSTRACT

The C-terminally Encoded Peptide (CEP) family of regulatory peptides controls root development in vascular plants. Here, we present the first NMR structures of CEP. We show that root-knot nematode (RKN: *Meloidogyne* spp.) also encodes CEP, presumably to mimic plant CEP as part of their stereotypic, parasitic interaction with vascular plants. Molecular dynamics simulations of plant- and nematode-encoded CEP displaying known posttranslational modifications (PTM) provided insight into the structural effects of PTM and the conformational plasticity and rigidity of CEP. Potential mechanisms of action are discussed with respect to the structure and sampling of conformational space. © 2013 Federation of European Biochemical Societies. Published by Elsevier B.V. All rights reserved.

1. Introduction

Plant peptide hormones, including CEP (C-terminally Encoded Peptides), are emerging as potent regulators of many plant developmental processes [1]. First identified and characterized in *Arabidopsis* by computational screens and mass-spectrometry, the precise role(s) of CEP ligands remains to be definitively elucidated [2]. It has been established that plant-parasitic nematodes, including cyst nematode (*Heterodera* spp., *Globodera* spp.) and root-knot nematode (RKN: *Meloidogyne* spp.) secrete peptides with striking sequence similarity to plant peptide hormones. It has been hypothesized that these molecules play a role in the formation of the novel plant cell types from which the nematodes feed, perhaps via molecular mimicry [3]. The breadth of communication between parasite and host is likely commensurate with the parasite's host range. Understanding this interaction will likely provide a powerful tool to examine the roles of endogenous pathways intrinsic to both host and parasitic biology.

Plant peptide hormones often exhibit post-translational modifications (PTM), thought to have roles in specifying peptide activity,

storage, or transport. PTM are known to affect conformation, alter binding abilities and specificity for target receptors. In particular, small cysteine-lacking plant peptide hormones undergo PTM, including proline hydroxylation (Hyp), hydroxyproline arabinosylation, and tyrosine sulfation [1]. Although, roles have yet to be ascribed for the majority of PTM of plant peptide hormones, a recent study detailed the requirement of hydroxyproline arabinosylation of *Lotus japonicus* CLE-RS2 in both function and receptor binding [4].

Ideally, biological activity could be deduced from a peptide's conformation, including its ability to sample alternate conformational states and the structural effects of PTM. To establish the role of PTM to plant and nematode encoded CEP, we characterized the structure of two CEPs: (1) CEP1 from the model plant host *Medicago truncatula* (MtCEP1) and (2) CEP11 from the plant parasitic nematode *Meloidogyne hapla* (MhCEP11). These two peptides showed significant sequence homology to *Arabidopsis thaliana* CEP1, which is responsible for root meristem maintenance [2]. Both *M. truncatula* and *M. hapla* have extensive genomic resources and are of great agricultural importance. Despite spanning just 15 amino acids, both peptides (MtCEP1 and MhCEP11) were found to exhibit defined structures, consistent with specific functional roles. We also show that the non-PTM peptides seem to retain a conformational rigidity compared to their PTM counterparts. Molecular

* Corresponding author at: Department of Plant Pathology, NC State University, Raleigh, NC 27695, United States. Fax: +1 919 515 9500.

E-mail address: bird@ncsu.edu (D. Mck Bird).

¹ These authors contributed equally to this work.

dynamics (MD) simulations demonstrated relative conformational plasticity and rigidity for specific MtCEP1 and MhCEP11 residues. This research lays the groundwork needed to specify residues critical to general receptor binding and also to differentiate the targeting of these peptides to particular receptors.

2. Materials and methods

2.1. CEP from RKN and vascular plants

Available genome resources for *M. hapla*, *M. incognita*, *M. chitwoodi*, *Caenorhabditis elegans*, *Globodera rostochiensis*, *Heterodera glycines*, *Pratylenchus coffeae*, and *Radopholus similis* were obtained from public repositories (www.ncbi.nlm.nih.gov and www.nematode.net), or were kindly provided by Dr. C.H. Opperman and Mark Burke. ORFs between 30 and 150aa were sampled from these sequences using the program getorf – EMBOSS package [5]. SignalP 3.0 was used to search each ORF for secretion signal sequences, using neural network and Hidden Markov Model modes [6,7]. ORFs that lacked a signal sequence or contained >5 cysteine residues were excluded from analysis. Using our deduced consensus sequence “xfrPTxpGxSPGxGx” based on the five initial Arabidopsis CEP, we interrogated our ORF database using a double-affine Smith–Waterman algorithm implemented in an accelerated TimeLogic hardware environment (TimeLogic DeCypher systems; www.timeLogic.com) [2,8]. Resulting matches were hand-curated to confirm match with the consensus sequence.

To acquire expression levels of *MhCEP*, RKN eggs, second stage juveniles, and induced galls were isolated from *M. truncatula* cv. Jemalong A17 3 weeks after inoculation and immediately frozen in liquid nitrogen. Total RNA was isolated from *M. hapla* and *M. truncatula* tissue using the RNeasy Mini Kit (Qiagen) and was processed for sequencing using standard Illumina protocols. TopHat and Bowtie were used to align reads to the source genome (i.e., *M. hapla* or *M. truncatula*) [9,10]. *M. hapla* CEP expression was measured as a percentage of all *M. hapla* CEP reads mapped or all *M. hapla* reads.

The active 15 amino acid ligand domains for MhCEP11 (AFRP-TAPGHSPGVGH) and MtCEP1 (AFQPTTPGNSPGVGH) were deduced from the appropriate genome sequence, and synthesized to >98% purity with the known modifications of hydroxylation of P4 and P11 [2]. Syntheses were performed by ChiScientific (Boston, MA, USA). Synthetic peptide purity was validated by mass-spectrometry and high-pressure liquid chromatography.

2.2. NMR spectroscopy

Experiments were performed on the hydroxylated-proline (residue 4 and 11) versions of the peptides using a 16.4 T spectrometer at controlled temperature (298.15 ± 0.1 K) on a Bruker Avance 700 MHz instrument equipped with TCI cryogenic probe. Peptides (4 mg/ml) were dissolved in 90% H₂O, 10% D₂O (v/v). DSS (4,4-dimethyl-4-silapentane-1-sulfonic acid) was used as an internal standard. Two-dimensional natural abundance ¹⁵N-heteronuclear single-quantum coherence (HSQC), ¹³C-HSQC, ¹H–¹H total correlation spectroscopy (TOCSY – 30 and 80 ms) and ¹H–¹H nuclear Overhauser effect spectroscopy (NOESY – 50 and 300 ms) spectra were recorded with standard pulse sequences and recycle delays of 3.0 s [11,12]. All spectra were processed with NMRPipe and analyzed with the NMRViewJ program [13,14].

2.3. Peptide structure determination

Using default parameters, ARIA (version 2.3) was used to perform structure calculations on the hydroxylated-proline (residue

4 and 11) versions of the peptides [15,16]. The 20 lowest energy structures from each iteration were used for NOE assignment and for each subsequent iteration. After eight iterations, the 20 lowest energy structures were refined by a molecular dynamics step in explicit solvent (water). From this, the 10 structures with the lowest energy were considered as accurately characterizing the peptide structures and are presented. Representation of the calculated structures were performed using PyMOL (The PyMOL Molecular Graphics System, Version 1.5.0.4 Schrödinger, LLC: www.PyMol.org).

2.4. Molecular dynamics simulation

MD simulations were performed with the GROMACS 4.4.5 software package using the AMBER 99sb-ildn force field and the flexible SPC water model [17]. The initial structures were immersed in a periodic water box of cube shape (1 nm thickness) and neutralized with counterions. Electrostatic energy was calculated using the particle mesh Ewald method. Cutoff distances for the calculation of the Coulomb and van der Waals interaction were 1.0 nm. After energy minimization using a steepest decent method, the system was subject to equilibration at 300 K and normal pressure for 100 ps under the conditions of position restraints for heavy atoms and LINCS constraints for all bonds. The system was coupled to the external bath by the Parrinello–Rahman pressure and temperature coupling. The final MD calculations were performed under the same conditions except that the position restraints were removed and the simulation was run for 50 ns. MD simulations were performed on the solved NMR structures of the hydroxylated-proline (residue 4 and 11) versions of the peptides as well as the modeled non-hydroxy-proline versions by removal of the OH group in PyMOL.

3. Results

3.1. CEP are found only in RKN and vascular plant genomes

CEPs were first described as a peptide hormone family restricted to plants. Our mining of the now much larger genomic datasets confirmed that observation with one notable exception, namely, the obligate plant-parasitic, root-knot nematodes including *M. hapla* also encode CEP. (Fig. 1). In no instance, including soybean- and potato-cyst nematode (*H. glycines* and *G. rostochiensis*), the migratory plant parasitic nematodes (*R. similis* and *P. coffeae*) or the free living *C. elegans*, were CEP genes detected. Apart from RKN, extensive computational analysis detected credible CEP genes in vascular plants only. The *M. hapla* CEPs were numbered in the order they appear in the genome, rather than on any perceived orthology to characterized plant peptide hormones.

Examination of the CEP-like proteins encoded by RKN and Medicago revealed, in addition to the CEP domain, a well-defined secretion signal sequence. In nematodes the cleavage site of the signal sequence is either immediately adjacent to the CEP domain (for MhCEP3, MhCEP6 and MhCEP7) or within a few amino acids of the ligand domain (Fig. 1). This is in contrast to plant CEP, which encode an obvious pro domain between the signal sequence and the ligand domain. As is the case for plant CEP, some RKN-encoded CEP have additional amino acids carboxyl to the 15mer active ligand (Fig. 1).

To confirm expression of RKN CEP, we independently sequenced the transcriptomes of 115 biological replicates of RKN-infected root tissue. Tissue collected 3 weeks after inoculation yielded more than 4.4 billion ESTs that could be mapped onto either the plant or nematode genomes. Additional transcriptome sequencing of *M. hapla* egg and second-stage larvae established that nematode CEP

including 100% of NMR assignable side-chain for MtCEP1 (Supplementary Table 3 and Figs. 1 and 2). There are inter-residue interactions observed throughout the full spectrum (0–12 ppm; red peaks do not exactly overlay black peaks) which lead to the >50 NOEs assigned for the structures.

The solved structures were obtained from a total of 50 or greater NOEs, have no NOE violations greater than 0.3 Å and display root mean square deviations (r.m.s.d) of ~1.5 Å over all backbone atoms (Table 1). Each peptide was characterized by nearly the same amount of inter-residue NOEs as intra-residue NOEs, ~25–30. Furthermore, both peptides have Ramachandran space for each residue >90% in generously allowed space or better. Superficially, the structures of MtCEP1 and MhCEP11 appear to be quite different. However, they do share several features, including beta turns at the amino- and carboxyl-termini and a structured core. Both peptides occupy similar volumes, indicative of well-defined structures (Fig. 2). The MhCEP11 peptide ensemble has the unique structural feature of a clearly defined alpha-helical character between residues 9–12. In comparison, MtCEP1 contains several beta-turns (residues 1–4, 6–9, and 10–13), and a perceived propensity of residues 8–13 to form alpha-helix (Fig. 2).

Data from this project are publically available from NCBI. For MtCEP1 and MhCEP11 structure, the PDB codes are 2mfo and 2mfm, respectively. For chemical shifts the BMRB codes are 19556 and 19555, respectively.

3.3. Molecular dynamics simulations of solved CEP structures

MtCEP1 and MhCEP11 were subjected to MD simulations in the following states to determine the structural implications of the PTMs: P4/P11, P4/Hyp11 and Hyp4/Hyp11. The radius of gyration (which measures overall structure compactness) and $C\alpha$ r.m.s.d were monitored throughout the simulation and described in detail after a 10 ns equilibration period (Fig. 3). The average $C\alpha$ r.m.s.d for MtCEP1 peptides were: 0.49 ± 0.04 , 0.59 ± 0.13 and 0.44 ± 0.09 nm for P4/P11, Hyp4/Hyp11, and P4/Hyp11, respectively. The average $C\alpha$ r.m.s.d for MhCEP11 peptides were: 0.46 ± 0.07 , 0.47 ± 0.12 and 0.56 ± 0.06 nm for P4/P11, Hyp4/Hyp11, and P4/Hyp11, respectively. The average radius of gyration for MtCEP1 peptides were: 0.66 ± 0.05 , 0.82 ± 0.11 and 0.72 ± 0.05 nm for P4/P11, Hyp4/Hyp11, and P4/Hyp11, respectively. The average radius of

Table 1
Details and statistics for quality assessment of peptide structures.

	MhCEP11	MtCEP1
Total NOES	50	58
Intra-residue	24	26
Inter-residue	26	32
<i>Average violations per structure</i>		
>0.3 Å	0	0
>0.1 Å	1.4	2.5
<i>Energy (kcal mol⁻¹)</i>		
van der Waals	-88.73 (±5.48)	-86.51 (±4.54)
Electrostatic	-409.61 (±44.75)	-515.14 (±16.55)
<i>Deviations from idealized geometry</i>		
Bond lengths (Å)	0.0036 (±0.0001)	0.0041 (±0.0003)
Bond angles (°)	0.564 (±0.036)	0.630 (±0.042)
Impropers (°)	1.47 (±0.23)	1.36 (±0.52)
<i>Ramachandran space</i>		
Core	61.1%	38.6%
Additionally	34.4%	50.0%
Generously	3.3%	9.1%
Disallowed	1.1%	2.3%
<i>RMSD (Å)</i>		
Backbone	1.751 (±0.724)	1.255 (±0.359)
Heavy atoms	2.437 (±0.621)	1.959 (±0.637)

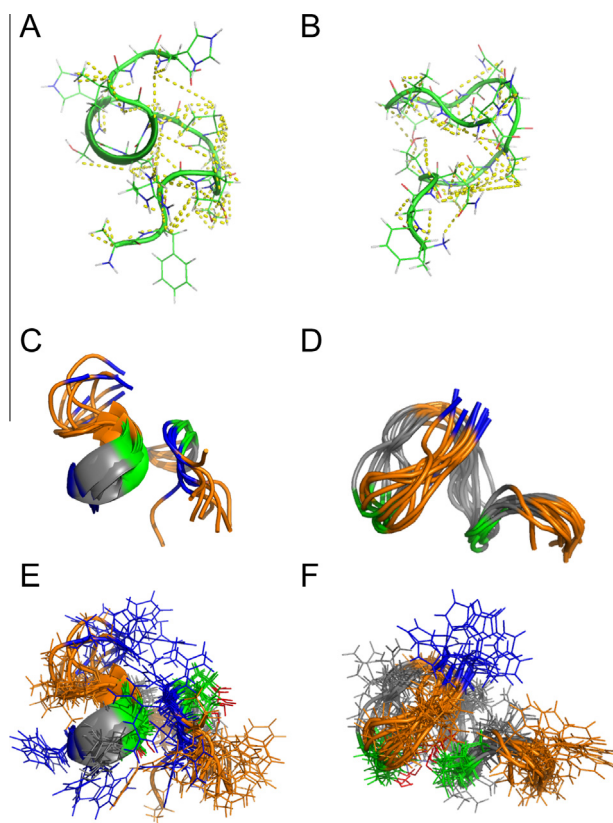


Fig. 2. Solution structures of MhCEP11 and MtCEP1. (A) and (B) represent the lowest energy structures and depict the NOE constraints (yellow lines) for MhCEP11 and MtCEP1, respectively. (C) Through (F) display the chemical characteristics of the solved peptides; hydrophobic residues are colored orange, hydroxy-proline residues are colored green and positively charged residues of Arginine and Histidine are colored blue. The 10 lowest energy structures are shown for MhCEP11 (C), and MtCEP1 (D), respectively. Panels E and F shows the same orientation as panels (C) and (D) but with lines drawn for the individual amino acids.

gyration for MhCEP11 peptides were: 0.69 ± 0.04 , 0.84 ± 0.10 and 0.84 ± 0.05 nm for P4/P11, Hyp4/Hyp11, and P4/Hyp11, respectively. These data show the conformational rigidity of P4/P11 and P4/Hyp11 (equilibrium met at ~10 ns for MtCEP1 and MhCEP11 – black and green lines Fig. 3) compared to the Hyp4/Hyp11 analogues.

4. Discussion

Receptor–ligand interactions are governed by several biophysical phenomena. Sequence is of clear importance. However, there are instances where receptors bind a diverse set of ligands [18], thus implicating a role for factors other than simply sequence in contributing to the interactions. In these cases, it is possible that receptors may accept ligands that exhibit a specific range of conformational plasticity. In this work we show that *M. truncatula* and *M. hapla* encode homologs of CEP in which in turn are homologous to those from *Arabidopsis* (Fig. 1) [1]. MtCEP1 and MhCEP11 have identical residues at 11 out of 15 positions (1, 2, 4, 5, 7, 8, 10, 12–15). These residues may be responsible for the determination of a global fold structural motif (Fig. 2) that a receptor will recognize. However, their movements in solution may also be critical to the interaction with the target as well. Because these movements may be defined and altered by the surrounding residues and/or PTM, we elected to perform structural and MD simulation studies which have provided a wealth of information on a structure to function standpoint.

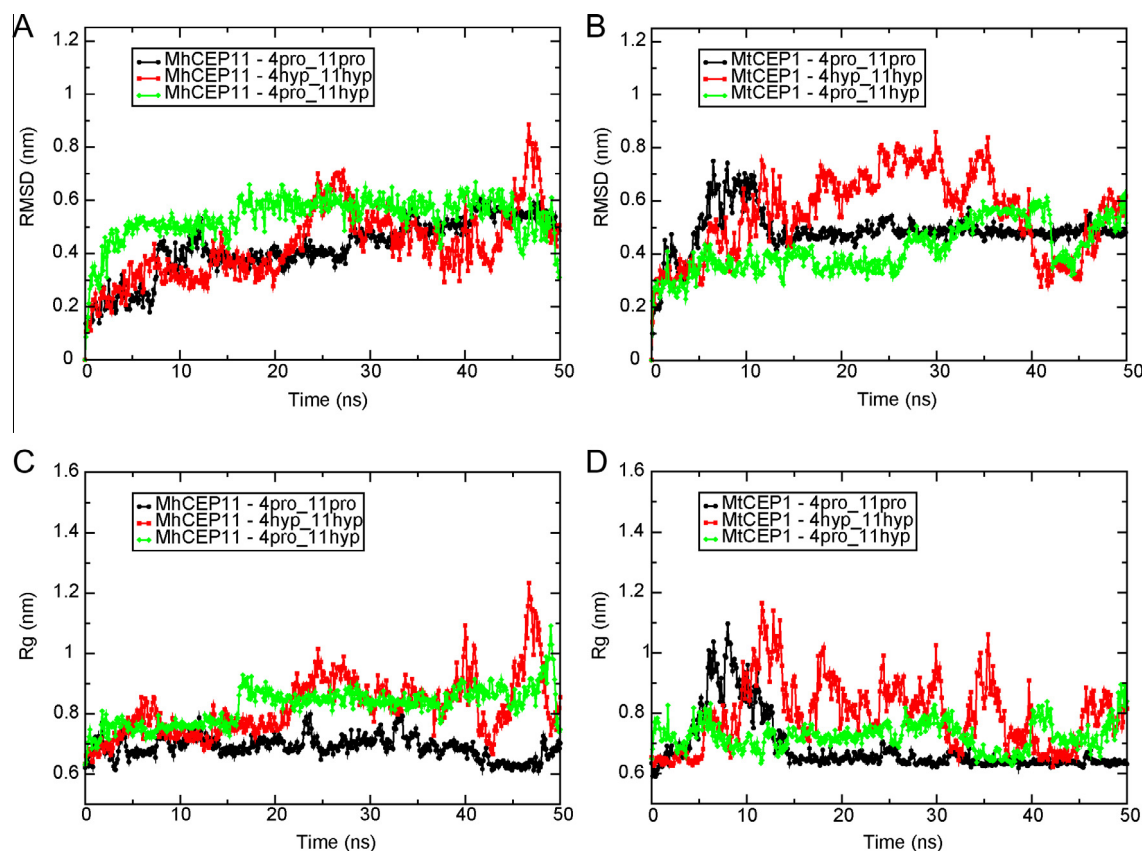


Fig. 3. C α r.m.s.d and radius of gyration analysis of the molecular dynamics simulation. Panels (A) and (B) shows the C α r.m.s.d of MhCEP and MtCEP peptides, respectively. Panel (C) and (D) show the radius of gyration of MhCEP and MtCEP peptides. In each panel, black lines represent P4/P11, green lines represent P4/Hyp11 and red lines represent Hyp4/Hyp11.

It is known that the CEP in *Arabidopsis* are posttranslationally modified at positions P4 and P11 to hydroxy-proline [2] and one or more of these modifications is necessary for storage, transport, or function. *Arabidopsis* CEP1 is responsible for root meristem development, among other phenotypes [2]. In *Arabidopsis*, mass-spectrometry studies of CEP have shown that P4 escapes hydroxylation in some instances, while P11 is always hydroxylated. Thus, although MhCEP11 and MtCEP1 are quite similar in sequence, the presence of PTM greatly changes the behavior of these peptides in solution. Overall, in both *M. truncatula* and *M. hapla*, the P4/P11 and P4/Hyp11 peptides are more restricted in their conformational plasticity compared to their Hyp4/Hyp11 counterparts (Fig. 3). This is evident in how quickly these peptides reach equilibrium during the MD simulations (~ 10 ns) in C α r.m.s.d and radius of gyration (black and green lines compared to the others). Furthermore, the surface area in the P4/P11 peptides is smaller when compared to their PTM counterparts, suggestive of a more compact structure (Supplementary Fig. 3). If PTMs are directly required for function, the PTM peptide presumably is able to sample a larger conformational space in-order to bind its receptor(s). Our MD simulations provided here show that this conformational plasticity is greatest when both P4 and P11 are posttranslationally modified to hydroxy-proline residues (Fig. 3).

Detailed analysis of the pairwise atom r.m.s.d plots from the MD simulations also revealed unique aspects of the effect of PTMs on the peptide's behavior in solution (Fig. 4). In particular, MhCEP11 in its various PTM states show that the hydroxylation of P11 leads to large movements in R3. In the non-PTM form, the ability of R3 sample conformational space is significantly reduced. We further observed that, when either P4 and P11 (or just P11) are

hydroxylated, the ability of non-hydroxylated P7 to sample conformational space also is restricted. PTM to MhCEP11 P4 and/or P11 also limit the conformational space potentially available to V13, although to a lesser degree. The impact of PTM on, the MtCEP1 peptides was less striking. For example, the presence of PTMs at positions 4 and/or 11 do not result in large conformational changes in Q3, the analogous position of R3 in MhCEP11. In fact, these modifications do have the opposite effect on P7, increasing the conformational plasticity of P7. Finally, these modifications at positions 4 and/or 11 result in a decrease in conformational plasticity of S10. We hypothesize that the observed differences in the ability to sample conformational space may limit the peptide's side chain atoms from making the necessary contacts with their respective targets. The differences in the conformational flexibility of the side chains between MhCEP11 and MtCEP1 could also indicate residues critical to specific function.

Assuming that either Hyp11 or Hyp4/Hyp11 modifications are necessary for function, there are several similarities and differences that may lead to the elucidation of distinct roles for RKN and plant CEP ligands. Like other small peptides, the MtCEP1 and MhCEP11 solution structures reveal residue side-chains that are quite dynamic (Fig. 2). The flexibility in the side chains is most evident in the amino- and carboxyl-terminal residues of each peptide. When these residues are removed from the r.m.s.d calculations, the r.m.s.d is reduced from 1.7 to 1.1 Å for MhCEP11, and from 1.2 to 1.0 Å for MtCEP1 (Fig. 2 and Table 1). This suggests that the cores of each peptide exhibit a stable backbone conformation whilst retaining the ability to sample conformational space in their side chains. Thus, we hypothesize that the general recognition properties are garnered through similar backbone structural motifs which

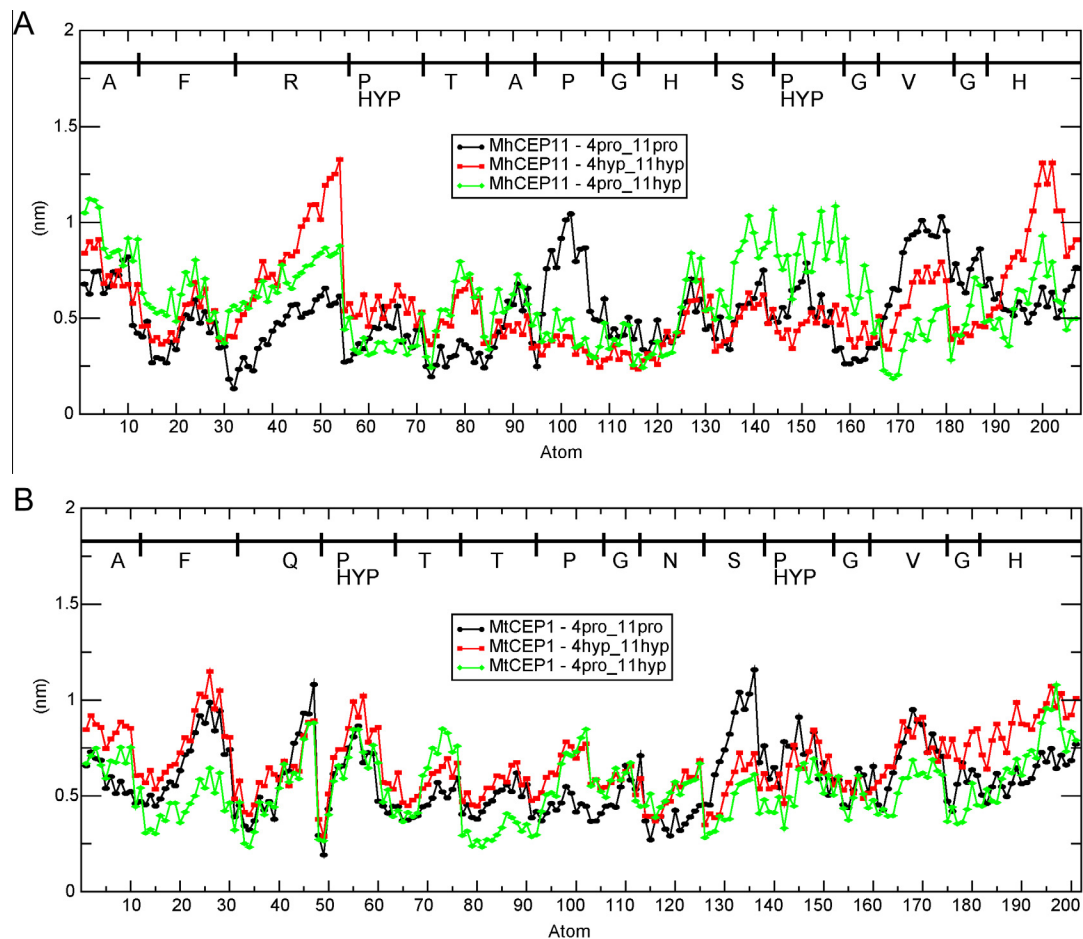


Fig. 4. Pairwise atom r.m.s.d. during the simulation. (A) MhCEP peptides. (B) MtCEP peptides. In each panel, black lines represent P4/P11, green lines represent P4/Hyp11 and red lines represent Hyp4/Hyp11. The peptide's sequence is noted above the curves. For positions 4 and 11 both P and Hyp are listed.

allow the side chains to position themselves in arrangements that allow for dynamic movement that could lead to specific functions for each peptide.

The receptors for the CEPs from *M. truncatula* and *M. hapla* are not currently known. In the absence of this information, probing the peptide's behavior in solution could provide details to its function. Genetic and other evidence implicate plant peptide hormones in the regulation of many processes in multiple tissues. Thus as a 11 member family of plant peptide hormones, *Medicago* CEP must sample a broad functional space. In contrast, as a parasite, RKN is under a different set of selection pressures that likely restrict the functional space of their CEPs to their restricted niche within the root vasculature. With this in mind, those similarities listed above might point to general mechanisms crucial for the formation of interactions with receptors. In contrast, differences (including the sequence in general) in the peptide's behavior in solution possibly suggest distinct mechanisms crucial for the interaction with specific receptors. There are slight differences in the α r.m.s.d in the Hyp4/Hyp11 PTM states (0.47 ± 0.12 vs 0.59 ± 0.13 nm, MhCEP11 vs MtCEP1, respectively) and P4/Hyp11 PTM states (0.56 ± 0.06 vs 0.44 ± 0.08 nm, MhCEP11 vs MtCEP1, respectively), which suggest slight difference in conformational plasticity (Fig. 3). Furthermore, investigation of the pairwise atom r.m.s.d over the simulation revealed unique aspects to each PTM, P4/Hyp11 and Hyp4/Hyp11 (Fig. 4). Specifically there are striking differences in the ability to sample conformational space when comparing Hyp4/Hyp11 MhCEP11 to MtCEP1 with regard to residues F2, R/Q3, P7 and G8. We propose that these residues could lead to the variability in receptor binding between *M. truncatula* and

M. hapla, with residues 8–15 responsible for the formation of the core general recognition properties (alpha-helical character). However, if P4 escapes hydroxylation, the most striking differences are seen around residues S10, Hyp11, and G12. The differences in residues critical to conformational plasticity between the hydroxylated states of CEP corroborate the role of PTMs in specifying function.

This research demonstrates the power of utilizing structural biology to characterize unique functions of individual members within large gene families. In particular, it helps to ameliorate many of the pitfalls associated with interpreting often what is pleiotropic, bioassay data [19]. Understanding the intersection of the biological space occupied by nematode and plant peptide hormone ligands will likely inform basic plant biology as well as nematode parasitism.

Acknowledgements

This work was supported in part by NSF Plant Genome Research Project: IOS 1025840 (D.M.B.), NSF Symbiosis, Defense and Self-Recognition Program: IOS-0840932 (D.M.B.), Australian Research Council's Grant ARC Grant (DP120101893 to N.I. and M.A.D.) and a USDA NIFA pre-doctoral fellowship award to PMD.

Appendix A. Supplementary data

Supplementary data associated with this article can be found, in the online version, at <http://dx.doi.org/10.1016/j.febslet.2013.10.033>.

References

- [1] Matsubayashi, Y. (2011) Post-translational modifications in secreted peptide hormones in plants. *Plant Cell Physiol.* 52, 5–13.
- [2] Ohyama, K., Ogawa, M. and Matsubayashi, Y. (2008) Identification of a biologically active, small, secreted peptide in *Arabidopsis* by in silico gene screening, followed by LC–MS-based structure analysis. *Plant J.* 55, 152–160.
- [3] Hewezi, T. and Baum, T.J. (2013) Manipulation of plant cells by cyst and root-knot nematode effectors. *Mol. Plant Microbe Interact.* 26, 9–16.
- [4] Okamoto, S., Shinohara, H., Mori, T., Matsubayashi, Y. and Kawaguchi, M. (2013) Root-derived CLE glycopeptides control nodulation by direct binding to HAR1 receptor kinase. *Nat. Commun.* 4, 2191.
- [5] Rice, P., Longden, I. and Bleasby, A. (2000) EMBOSS: the European molecular biology open software suite. *Trends Genet.* 16, 276–277.
- [6] Bendtsen, J.D., Nielsen, H., von Heijne, G. and Brunak, S. (2004) Improved prediction of signal peptides: SignalP 3.0. *J. Mol. Biol.* 340, 783–795.
- [7] Nielsen, H., Engelbrecht, J., Brunak, S. and von Heijne, G. (1997) Identification of prokaryotic and eukaryotic signal peptides and prediction of their cleavage sites. *Protein Eng.* 10, 1–6.
- [8] Smith, T.F. and Waterman, M.S. (1981) Identification of common molecular subsequences. *J. Mol. Biol.* 147, 195–197.
- [9] Trapnell, C., Pachter, L. and Salzberg, S.L. (2009) TopHat: discovering splice junctions with RNA-Seq. *Bioinformatics* 25, 1105–1111.
- [10] Langmead, B., Trapnell, C., Pop, M. and Salzberg, S.L. (2009) Ultrafast and memory-efficient alignment of short DNA sequences to the human genome. *Genome Biol.* 10, R25.
- [11] Wüthrich, K. (1986) *NMR of Proteins and Nucleic Acids*, Wiley, New York.
- [12] Bax, A. and Davis, D.G. (1985) MLEV-17-based two-dimensional homonuclear magnetization transfer spectroscopy. *J. Magn. Reson.* 65, 355–360. 1969.
- [13] Johnson, B.A. (2004) Using NMRView to visualize and analyze the NMR spectra of macromolecules. *Methods Mol. Biol.* 278, 313–352.
- [14] Delaglio, F., Grzesiek, S., Vuister, G.W., Zhu, G., Pfeifer, J. and Bax, A. (1995) NMRPipe: a multidimensional spectral processing system based on UNIX pipes. *J. Biomol. NMR* 6, 277–293.
- [15] Rieping, W., Habeck, M., Bardiaux, B., Bernard, A., Malliavin, T.E. and Nilges, M. (2007) ARIA2: automated NOE assignment and data integration in NMR structure calculation. *Bioinformatics* 23, 381–382.
- [16] Linge, J.P., Habeck, M., Rieping, W. and Nilges, M. (2003) ARIA: automated NOE assignment and NMR structure calculation. *Bioinformatics* 19, 315–316.
- [17] Pronk, S. et al. (2013) GROMACS 4.5: a high-throughput and highly parallel open source molecular simulation toolkit. *Bioinformatics* 29, 845–854.
- [18] Holton, N., Cano-Delgado, A., Harrison, K., Montoya, T., Chory, J. and Bishop, G.J. (2007) Tomato BRASSINOSTEROID INSENSITIVE1 is required for systemin-induced root elongation in *Solanum pimpinellifolium* but is not essential for wound signaling. *Plant Cell* 19, 1709–1717.
- [19] Strabala, T.J. (2008) CLE genes in plant development: gain-of-function analyses, pleiotropy, hypermorphology and neomorphy. *Plant Signal. Behav.* 3, 457–459.